6th European Conference on Computational Mechanics (ECCM VI)
7th European Conference on Computational Fluid Dynamics (ECFD VII)
June 11–15, 2018, Glasgow, UK

HEAT TRANSFER DEPENDENT ORIFICE JET FLOW OF A THERMO-VISCOUS SHEAR-THINNING FLUID

Markus Rütten⋆

⋆German Aerospace Center, Bunsenstrasse 10, 37073 Göttingen, Germany
markus.ruetten@dlr.de

Key words: *Thermo-viscous flow, shear thinning, Carreau fluid, heat transfer*

Non-Newtonian fluid properties can change the flow behaviour and the resulting flow topology significantly, even for low Reynolds number laminar flows. The prediction of the flow field is even more difficult when thermal effects come into play. In particular, when high shear rates occur and different temperatures act on the fluid changing its viscosity significantly, symmetry breaking is an often observed flow phenomenon. A well known flow case, which is the focal point of this study, is the laminar orifice jet flow of a thermo-viscous shear thinning fluid through a straight duct. Isothermal flows of Newtonian fluids reveal a straight jet flow leaving the orifice, in contrast to isothermal non-Newtonian fluid flows, which show a deflection of the orifice jet and complicated flow separation and attachment structures within the duct. In the present CFD study wall temperature dependent flow structures are investigated for the flow of a Carreau fluid through a duct with an orifice. The temperature dependence of the fluid viscosity is modelled by applying the standard Williams-Landel-Ferry (WLF) equation. It is shown that thermal viscous shear-thinning due to high shear rates and increased wall temperatures at the duct walls lead to a significant decrease of viscosity of three orders of magnitude in the near-field of the orifice. Locally reduced viscosity can be used to control the jet flow behaviour. In the present simulation campaign thermal boundary conditions are varied over a wide range in order to derive relations between heat transfer, non-Newtonian fluid properties and the behaviour of the orifice jet flow.

1 Introduction

Non-Newtonian fluids reveal a wide variety of properties due to their non-linear behaviour of viscosity in shearing flows. Since these types of fluids are widely used in technical, industrial and medical applications and also occur in biological flows, the knowledge about their complex properties and flow behaviour is necessary for the design of novel devices. The complex flow behaviour is caused by their molecular composition. Long entangled molecular chains lead to higher viscosities. High shear flow rates can tighten and align the molecular chains which leads to a decrease of the shear viscosity. This effect is called shear-thinning. The resulting flow phenomena of these processes are not easily to predict, in particular in complex flow applications

[5], [7]. The flow prediction is even more difficult when additional thermal loads are playing a significant role, since middle and high-molecular-dense fluids are sensitive to temperature influences on the viscosity [38]. Thus, heat transfer at walls, its effect on the nonlinear viscosity and the resulting flow phenomena are a main focal point in the research field of non-Newtonian fluids [6], [32], [19]. In particular, heat exchanger, lubrication systems or oil cooler are technical application in which the properties of non-Newtonian fluids are essential for the design and layout. Numerical simulations, conducted during the design process of such applications, are based on very accurately described fluid models [28]. Therefore, experimental and numerical studies are necessary to capture all phenomena which are related to thermal viscosity properties of non-Newtonian fluids, in particular when contraction and expansion flows are investigated. Both flow categories are combined in orifice flows.
A classical validation test case for Newtonian and non-Newtonian fluids is the contraction flow: suddenly the channel height or pipe diameter is significantly reduced. Owens [28] elaborately referred about a manifold of numerical and experimental work addressing different types of non-Newtonian fluids and configurations. Rodd [29] classified the observed flow phenomena with regard to separation, vortices and instabilities. The spatial extension of corner vortices, the location of separation and attachment points are investigated in dependence on fluid type, Reynolds number and geometrical aspect ratios of the flow configurations. In many investigations the contraction ratio of $4:1$ is chosen, [37], [26]. Focal point of latest research work are flow effects which can be observed for Boger and visco-elastic fluids[17], [1]. However, shear-thinning and shear-thickening pseudo-plastic fluids are investigated as well. For this study, in particular the research work of Cogswell [12] [13] is of interest, since low and middle density polymers are considered, a fluid category, which reveals shear-thinning viscosity properties.
There are a lot of investigations covering expansion flows of both Newtonian and non-Newtonian fluids. Interestingly validation test cases concentrate on the 1:3 expansion ratio, which was experimentally investigated by Durst [15], who could observe asymmetric flow behaviour for symmetric duct configurations for Newtonian fluids and certain flow conditions. Based on experimental and numerical results a bifurcation diagram was derived: a lower Reynolds number limit exists, under which two symmetric corner vortices occur. But if a certain higher Reynolds number is exceeded, a symmetry breaking of the jet like flow can be observed, whilst one vortex is growing, the other is shrinking. The onset of this asymmetric flow is called pitchfork bifurcation. Also a second bifurcation occurs: with a further increase of the Reynolds number beyond the next critical limit a third vortex arises. Although Cherdron [11] conducted a series of experiments varying the expansion ratio and, of course, the Reynolds number, again for Newtonian fluids, but still, it is controversial at which Reynolds numbers theses bifurcations occur. Fearn [18] could prove the first bifurcation at a Reynolds number of $40,5$ and 1:3 expansion, whereas Durst reported a bifurcation Reynolds number of 112 [15]. In order to clarify that Drikakis [14] conducted numerical simulation and extensive parameter studies for a planar configuration, found bifurcation Reynolds number in the same range. However, to experimentally determine the bifurcation Reynolds numbers accurately is challenging: to realise pure two-dimensional flows is quite difficult due to the need of limiting boundaries. Further uncertainty stems from the initial inflow, small disturbances are able to cause asymmetrical flows. Battaglia et al. [4] conducted experiments with quasi-two-dimensional rectangular channel configurations, bifurcation was observed for Reynolds numbers in the range of 150 to 600.
Neofytou [25] investigated the sudden expansion flow for different non-Newtonian fluids, the

flow of Power-Law, Casson and the Quemada fluids were simulated, concentrating on the pitch-fork bifurcation effect. Ternik [33] numerically scrutinised the planar 1:3 expansion flow with special attention to shear-thinning effects of generalised Newtonian fluids. In comparison to Newtonian fluids shear-thinning exhibits a substantial impact on the bifurcation Reynolds numbers [33]. In particular, the size of the corner vortices are significantly different in comparison to Newtonian fluids [34]. Even the flow regime might change: in case of Newtonian fluids the flow seems to remain steady, though this is a point of discussion, shear-thinning non-Newtonian fluid flows appear to faster develop transient behaviour.
The orifice flow is a combination of both contraction and expansion flows, with the orifice plate as linking element. Special attention is paid to orifice flows since this type of flow occurs in a lot of technical applications such as valves, orifices or even orifice flow meter. Greenspan was one of the first, who numerically investigated orifice flows [20]. Over time this flow type has become a validation case for numerical simulation tools, see [26]. Of particular interest is the orifice flow meter. In case of Newtonian fluids quite simple relationships exist between flow rates and pressure losses [21], [2]. Guidelines for engineers have been derived, see for instance [16]. More complicated are the non-Newtonian flow cases [31]. Those relationships are still topic of investigations: Valle et al. [35] numerically simulated the flows of purely viscous Power-Law fluids for a wide range of the associated power-law index. It was found found that a unique master curve can be obtained by plotting the Euler number versus the generalised Reynolds number. Rothstein et al. [30] investigated the extensional flow of a polystyrene Boger fluid through an orifice of a 4:1:4 axisymmetric contraction/expansion configuration, observing viscoelastic flow properties. Most of those studies, however, concentrated on flow topology alternation, flow regime change or some other transient effects. The impact of heat transfer is not well investigated so far, therefore, the focal point of this study is the orifice flow of a thermo-viscous shear-thinning Carreau fluid under specific thermal boundary conditions.

2 The Non-Newtonian Fluid and the Simulation Setup

In contrast to Newtonian fluids, the properties of non-Newtonian fluids play a significantly more important role in shearing flows due to their ability to change their viscosity over orders of magnitude in dependence of local shear rates. If thermal loads also play a role, then heat transfer can enforce the viscosity change of those fluids even more. Thus, the accurate modelling of the non-Newtonian fluid properties of the considered thermo-viscous shear-thinning fluid is crucial for the description of such type of flow problems, which is demonstrated in the present simulation campaign. Fluid viscosity modelling together with a suitable CFD grid and a strict numerical simulation strategy is a precondition for reliable simulation results.

2.1 Properties of the Non-Newtonian Carreau Fluid

Although the flow case of a Newtonian fluid with a constant viscosity of $\mu = 100Pas$ is also considered in order to have a reference case, we concentrate on a specific class of non-Newtonian fluids: the thermo-viscous shear-thinning fluids without any yield stress or temporal

relaxation properties. Both the temperature T and the shear rate, $\dot{\gamma} = \sqrt{\frac{1}{2}[\mathbf{D} : \mathbf{D}]}$, have an impact on the viscosity of the these non-Newtonian fluids. The simplest type of the considered shear-thinning fluid is the Ostwald - de Waele fluid [27], whose viscosity is modelled by a power law, therefore, it is also called Power-Law fluid. However, flow models purely based on the power law have the model limitation that they do not possess any lower and upper viscosity restrictions. This leads to fluid modelling errors at very low and very high shear rates, where the shear dependent viscosity reaches unrealistic values. Moreover, numerical simulations reveal that Power-Law fluids show worse convergence rates, in particular in flow regions, in which the second invariant I_2 of the strain tensors $\mathbf{D} = \frac{1}{2}\left(grad\vec{v} + grad\vec{v}^T\right)$ is small, as, for example, in nearly uniform flows.

An alternative to a Power-Law fluid is the Carreau fluid model [8], which has the advantage to have both a constant zero viscosity and a constant infinite viscosity. These model limitations reflect the properties of real fluids very well [5]. The flow curve of a Carreau fluid is calculated by using (1),

$$\eta = \eta_\infty + (\eta_0 - \eta_\infty)\left\{1 + (\lambda\dot{\gamma})^2\right\}^{\frac{n-1}{2}} \quad , \tag{1}$$

in which n is the flow index, η_0 the lower limit or zero viscosity, η_∞ the upper limit or infinite viscosity and $\dot{\gamma}$ the generalised shear rate. The parameter λ controls the transition from the Newtonian to the non-Newtonian behaviour. This parameter can be determined by the characteristic stress τ_γ, at which the deformation behaviour of the fluid changes: $\lambda = \eta_0/\tau_\gamma$. In principle this time constant is the reciprocal value of the critical shear rate $\dot{\gamma}_c$, at which exceeding shear rates start to reduce the viscosity of the fluid. In this simulation study we used the following fluid parameters, $n = 0.2$, $\lambda = 0.5s$, $\eta_0 = 100Pas$, $\eta_\infty = 0.001Pas$, which are describing the fluid properties valid for a reference temperature $T_{ref} = 403.15K$. The associated flow curve is depicted in Fig. 1. The small values of the time constant and the flow index are consciously chosen in order to achieve a high sensitivity of the fluid viscosity in particular to lower shear rates, so that the viscosity can drop orders of magnitudes over the full range of the expected flow shear rates. This is not non-physical, since low-density polymers, carbon and silicone oils or especially synthesised engine oils just reveal such fluid properties.

Modelling thermal-viscosity is a research field of its own: as many non-Newtonian fluid models as many temperature dependent viscosity models exist. However, there is an experimental observation that for a certain group of non-Newtonian fluids, low and high density polymers or certain silicone oils, a change of the global temperature level only leads to a shift of the flow curve, whereas the principle shape of the known flow curve at a certain temperature is barely changed. This observation has led to a certain modelling concept: a so called *master flow curve* is measured for a reference temperature, thereafter, this master flow curve is adapted to the new temperature level by a viscosity-temperature shift factor a_T. This shift factor is called time-temperature superposition parameter, following the notation of [38], sometimes it is also called Andrade factor [3]. Now modelling the temperature influence on the viscosity is reduced to determine this factor. Different equations can be applied to this problem. In this work the so-called *William-Landel-Ferry equation*, in short *WLF-equation* is used to determine the viscosity-temperature shift factor, now called WLF shift factor [38], [19]. The WLF-equation reads as follows:

$$log\left(a_T\right) = log\left(\frac{\eta(\dot{\gamma}, T)}{\eta(\dot{\gamma}, T_{ref})}\right) = \frac{-C_1\left(T - T_{ref}\right)}{C_2 + \left(T - T_{ref}\right)}\,. \tag{2}$$

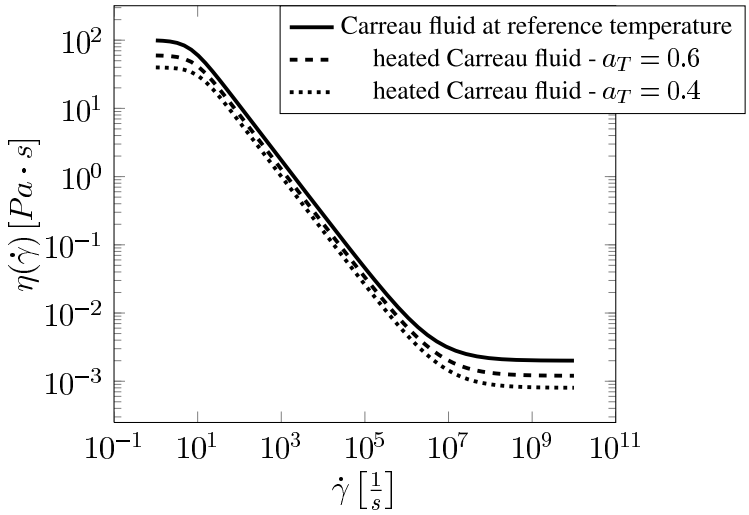

Figure 1: Fluid curves for a Carreau fluid model, $n = 0.20, \lambda = 0.5s$, $\eta_0 = 100Pas$, $\eta_\infty = 0.002Pas$, at the reference temperature, and for temperatures leading to viscosity-temperature shift factors of 0.6 and 0.6.

In this equation, T_{ref} is the reference temperature, for which, in this study, a value of $403.15K$ is assumed. The fluid parameters C_1 and C_2 have to be determined experimentally for each non-Newtonian fluid, however, for polymers the commonly used and experimentally determined values are $C_1 = 8.86$ and $C_2 = 101.6K$. These values are also used in the present simulation campaign. Eventually, the thermal-viscosity model has to be combined with the Carreau fluid model equation, which finally leads to:

$$\eta\left(\dot{\gamma}, T\right) = a_T \eta_\infty + \frac{a_T(\eta_0 - \eta_\infty)}{\left(1 + (a_T \lambda \dot{\gamma})^2\right)^{\frac{1-n}{2}}}\,, \tag{3}$$

Equation (3) was implemented in the DLR THETA code for the performed simulation campaign.

2.2 The Channel - Orifice Flow Configuration, the CFD Grid and Simulation Setup

The considered flow channel with its integrated orifice plate is a very simple configuration: It consists of an inflow and outflow channel separated only by an orifice plate of a thickness of D. Since the orifice has a height of $2D$, the orifice/pipe ratio, β, is 0.5, the aspect ratio of the orifice, γ, is also 0.5. The orifice is symmetrically placed on the channel longitudinal axis. The inflow channel has a length of $17.5D$, the outflow channel is $24.5D$ long. Both channels have a height of $8D = 0.02m$. A sketch of the configuration is depicted in Fig. 2.
For the present numerical simulation study a suitable flow domain has to be generated addressing different categories of flow types. At the walls the developing thermal and momentum boundary layer flows have to be well resolved. However, more essential for the simulation of such flows is to pay special attention to the corners. Here a very fine spatial grid resolution has to be realised in order to capture all flow phenomena of the corner and vortical flows. At the channel corners vortices are expected and jet like flows within and behind the orifice. The latter

shall be affected by flow separation at the orifice corners. Thus, very smooth grid cell topologies and slow growing grid element aspect ratios are basic prerequisite for the used CFD grids. For the generation of the CFD grid the commercial mesher "Centaur" from the company Centaur-Soft [10] has been applied. It has to be remarked that the used flow solver can only to run on three dimensional grids, for two dimensional cases a so called quasi-two-dimensional approach is implemented, which means that a two dimensional CFD grid has to be extended in such a way in the third direction that a one-cell layer is build. In the present case the a one-cell thickness is $0.25D$. Even though the memory requirement is slightly higher, there is no special 2D CFD grid treatment necessary, which substantially simplifies the programming and handling of the used CFD code. After an extended grid study the CFD simulation campaign has been conducted on a quasi-two-dimensional hybrid grid consisting of hexahedral and prismatic volume elements and associated surface triangles and quadrilaterals at the boundaries. The grid consists of 330530 grid points, 189552 prisms, 69156 hexahedrons, 379104 triangles and 140976 quadrilateral grid cells. The hexahedrons are building the structured grid closed to the wall, which consists of 32 layers. This high layer number is necessary for resolving both, the momentum driven boundary layer flow and also the thermal boundary layer. In order to capture the velocity profile slopes accurately the first wall normal cell height is in average $0.02D$, the associated growth rate in wall normal direction is 1.12. The overall height of the hexahedral stacks are varying since the grid has to be locally adapted i.e. to be able to resolve vortical flow structures in corner regions, the so-called Moffatt vortices [24]. In Fig. 2 details of the grid cell topology are illustrated. It is obvious that no use is made of intrinsic symmetry features of the flow configuration: The grid is consciously not symmetrically built, instead the present hybrid structured - unstructured grid approach is chosen to intend to trigger small disturbances by grid asymmetry.

The setup of the flow simulation starts with the boundary conditions: At the inflow boundary of the channel a plug flow with a constant velocity of $3.2m/s$ has been predefined, the inflowing fluid has the reference temperature of $403.15K$. Consequently, the fluid density is $1000\frac{kg}{m^3}$ and the zero viscosity $100Pas$. In this study the channel height of $0.02m$ is taken as reference length. Using these parameters leads to the initial channel Reynolds number of $Re_c = 0.64$ at the inflow boundary. For a constant viscosity the orifice Reynolds number is $Re_o = 0.16$. At such a low Reynolds number flow condition it is not expected that the creeping Newtonian fluid flow shows asymmetries when flowing through the orifice plate. At the channel outlet simple outflow boundary condition has been set. All other parts have been modelled as no-slip viscous walls. During the present simulation campaign both the thermal boundary conditions at the upper and lower channel walls behind the orifice plate have been varied in order to show the impact of a changed heat transfer on the flow behaviour of the thermo-viscous shear-thinning fluid. The simulation results for the isothermal and thermo-viscous shear thinning Carreau fluid flow are compared with those of the pure Newtonian fluid.

The numerical simulations have been performed on a desktop computer using the DLR THETA code [22] for solving the incompressible Navier-Stokes equations. This finite volume code is a variation of the DLR standard flow solver TAU. A dual grid approach is applied to unstructured hybrid grids, all flow variables are stored at the same location, the so-called collocated respectively non-staggered grid approach. An efficient coupling of the velocity and the pressure fields is ensured by using the Chorin projection method or the SIMPLE algorithm, see [36]. For spatial discretisation different variations of 1st or 2nd order upwind methods as well as 2nd order central schemes can be used. Here a mixed 2nd order scheme has been chosen combined with

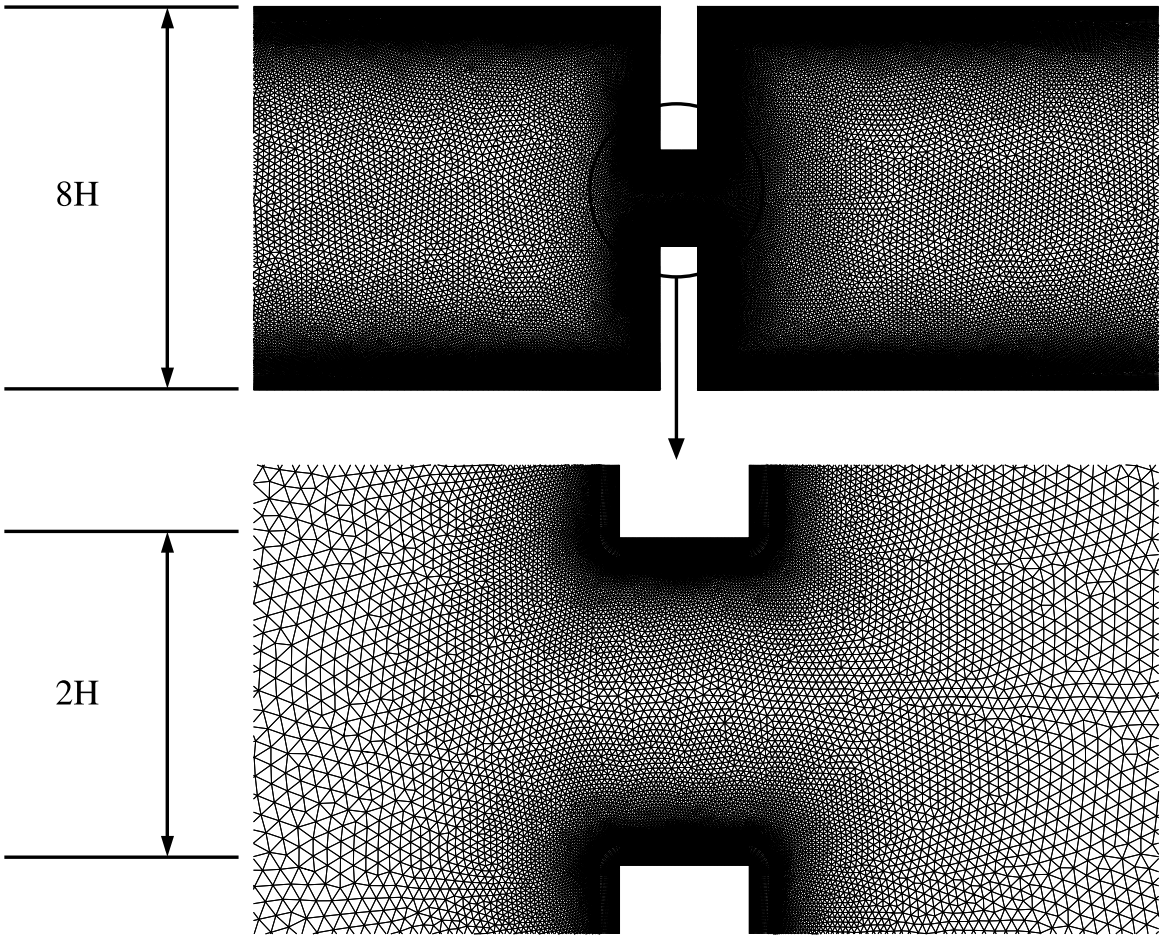

Figure 2: Grid topology of the flow channel with the orifice plate and enlarged grid details

a special correction algorithm in order to get very smooth data for calculation of derived vector fields. The well-known checkerboard instability of the pressure is eliminated by a 4th order stabilisation term, which is added to the left and the right hand side of the Poisson equation. A matrix-free formulation is used for solving the linear equations. This formulation reduces the memory requirements of the code considerably. A variety of multi-grid methods ensure efficient solutions of the linear equations, even on fine grids. Domain decomposition is used as parallelisation concept. The parallel efficiency is high on desktop computers with only a few CPUs as well as on massive parallel systems with thousands of CPUs. The code is well validated by a variety of experimental and numerical validation campaigns and is state of the art in regard to performance, efficiency and accuracy [22] . In the considered flow case a $4-w$ multi-grid cycle has been performed to accelerate the CFD calculations. The projection method has been used for the unsteady calculation, in which the time-step has been set to $0.001s$, resulting in grid cell CFL numbers less than one. The three point backward scheme, a variation of a BDF2 scheme, has been used for temporal discretisation.

3 Analysis of the Channel Orifice Jet Flows

The analysis of the simulation results starts with the investigation of the isothermal orifice jet flow within the channel. At first the case of the shear independent Newtonian fluid flow is considered. The flow topology is compared with the flow simulation results of the Carreau fluid. In the second part of the analysis, the temperature dependency of the viscosity is taken into account, and the flow topologies of the Newtonian and non-Newtonian fluid are investigated. The last part concentrates on the possibility to control the flow behaviour by changing the viscous properties of the Carreau fluid. The analysis of the flow simulation results is based on contour plot of colour-coded quantities of interest and the so called line integration convolution technique (LIC) [9], which is used to visualise flow structures by a kind of areal streamline line technique.

3.1 The Isothermal Orifice Jet Flows

The isothermal Newtonian and Carreau fluid flow cases are considered as reference. It is assumed that not only the walls and the incoming fluid have the same temperature, but also that the viscosity is temperature independent, that means, that even the locally generated heat, which is a product of dissipation due to high shearing rates, is not taken into account for changing the viscosity. At first the orifice flow of the Newtonian fluid is considered, illustrated in figure 3.

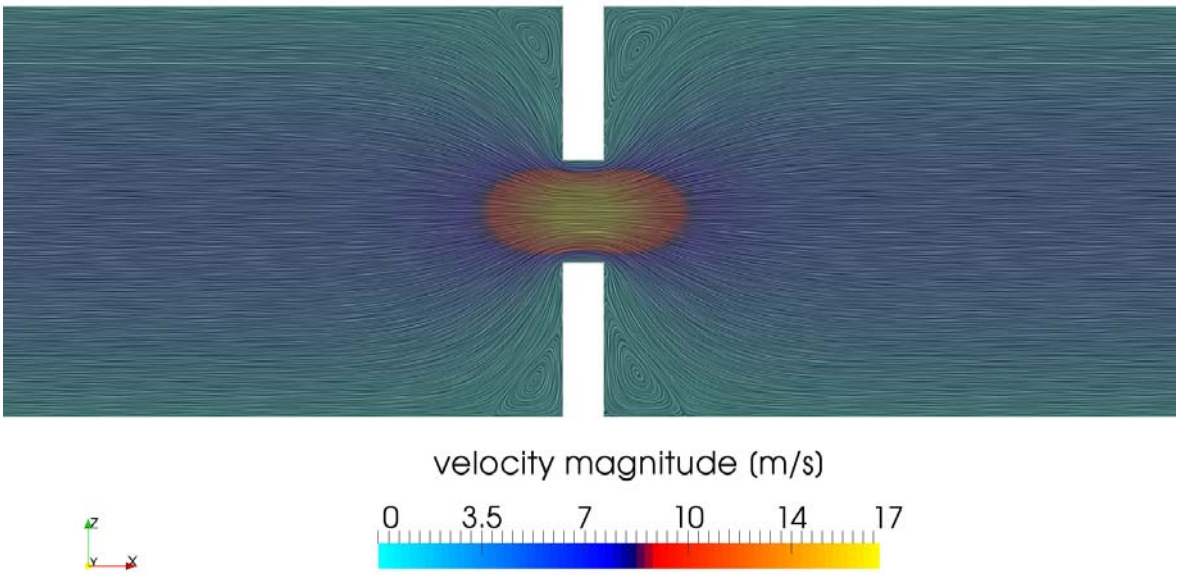

Figure 3: Orifice flow of the Newtonian fluid, flow field visualised using LIC applied to the velocity field, contour plot of the colour-coded velocity magnitude

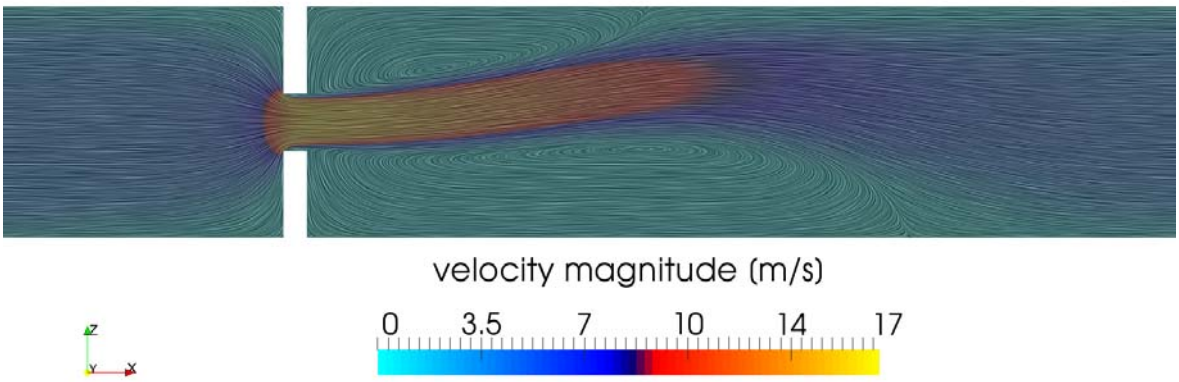

Figure 4: Orifice flow of the shear-thinning Carreau fluid, flow field visualised using LIC applied to the velocity field, contour plot of the colour-coded velocity magnitude

The depicted line integration convolution of the velocity field shows a flow topology, which is nearly symmetrical to the longitudinal axis of the channel, as is typical for Newtonian fluids at that low Reynolds number. In relation to the middle cross section of the orifice plate the symmetry is broken: The separated, vortical flow structures upstream of the orifice are smaller than the depicted Moffatt corner vortices behind the orifice. This is a result of momentum and shear effects, and, of course, of the small Reynolds number. The latter is not zero, thus shearing effects at this high viscosity level can accumulate which eventually leads to the observed flow topology symmetry changes. Besides that, the resulting flow show a further typical sign for Newtonian flows: the Moffatt corner vortices reveal quite straight outer vortex border, which is often reported for such a low Reynolds number. Outward curved vortex borders are not expected until the Reynolds number exceeds certain values, depending on the orifice aspect ratio β, in this case for $\beta = 0.5$ and $\gamma = 0.5$ the limit is round about $Re_o = 12$, see [26] and [34].
Now, the Carreau fluid flow case is considered. Details of the flow topology can be observed in figure 4, again the velocity field is illustrated by the LIC algorithm, additionally the velocity magnitude is colour coded in order to highlight the jet flow region. In contrast to the Newtonian flow case the flow simulation result for the Carreau fluid reveal a strong and dominant asymmetric orifice jet flow along the longitudinal axes. This jet flow is slightly constricted and does not spread as fast as in the Newtonian flow case. As a result the Moffatt corner vortices respectively the vortical separation bubbles behind the orifice are differently elongated, of course due to the deflection of the jet. Besides the deflected orifice jet flow and its impact on the Moffatt vortices behind the orifice, another essential flow feature caused by the shear-thinning fluid properties of the Carreau fluid is visible: it is the complete absence of the Moffatt corner vortices in front of the orifice. This flow behaviour is typical for the chosen Carreau fluid parameter set and it is well described by Niedziella [26].
As mentioned above this flow phenomenon, reflected by the present flow simulation, is well known from studies of expansion flows. In the present case the unstructured - structured hybrid grid approach is able to enforce relevant asymmetries in the flow so that this symmetry breaking occurs without the usage of any additionally superposed disturbances, as are often necessary,

in particular, in case of highly symmetric structured grids. The latter is an essential reason why often three-dimensional unstructured grid approaches are chosen. In fact, 3D unstructured grids seem to damp disturbances more efficient in comparison to 2D grids, but not so strong that relevant disturbances, leading to symmetry breaking of the flow topology, are prevented from growing. In fact, it has been observed that in case of unstructured 3D grids it is not necessary to provoke a breaking of the flow topology symmetry, in contrast 2D grid approaches need a lot more iterations to reveal such kind of flow phenomena observed in experiments. In this study it cannot be clarified finally, what the best grid strategy for such flows might be. This, of course, depends also on the chosen flow solver and order parameters of the flow problem itself, hence, more studies have to be done in future to address that point. This uncertainty, however, enforces the researcher to validate the numerical simulation results with experimental data.

In figure 4 the LIC visualisation also reveals that the associated vortex centres are shifted to-

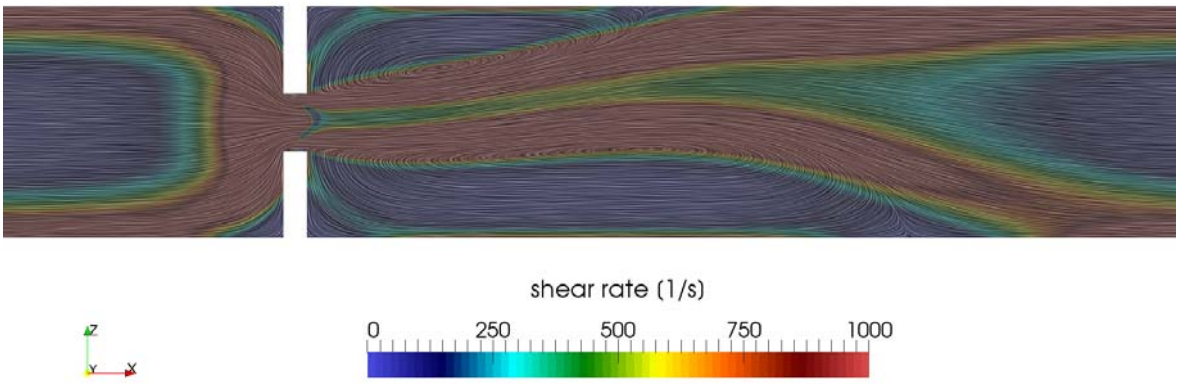

Figure 5: Orifice flow of the shear-thinning Carreau fluid, flow field visualisation using LIC applied to the velocity field, contour plot of the colour-coded shear rate

wards the dominant jet flow. Shear-thinning is the reason for that, which can be proven when observing the the effective, local shear rate shown in figure 5. The resulting local viscosity is illustrated in 6 as colour plot, the LIC visualisation facilitates the flow structure assignment. In the inflow region, where the flow profile has a plateau like shape, and in the corner regions, where the flow is nearly fading out, a local viscosity close to the zero-viscosity is found. In the wall near regions of pure shear flow and flow regions with high accelerations, in particular at the vortical flow regions closer to the walls the strong shear-thinning effects can be observed. Between these high shear regions the viscosity nearly reaches the zero-viscosity level. That symmetry breaking can occur for such a low initial reference Reynolds number seems to be astonishing at the first glance, however, looking at the local Reynolds numbers, which is calculated with the constant channel height but with the varying local dynamic viscosity, can help to explain the observed flow phenomenon, see figure 7. The initial Reynolds number is far away from any values at which asymmetries could be triggered by some disturbances, they would be damped out as it is the case for the Newtonian fluid where the Reynolds number is constant and low. In contrast, the shear-thinning property of the Carreau fluid leads to an increase of the local Reynolds number of orders of magnitude, in particular at the orifice and the jet flow

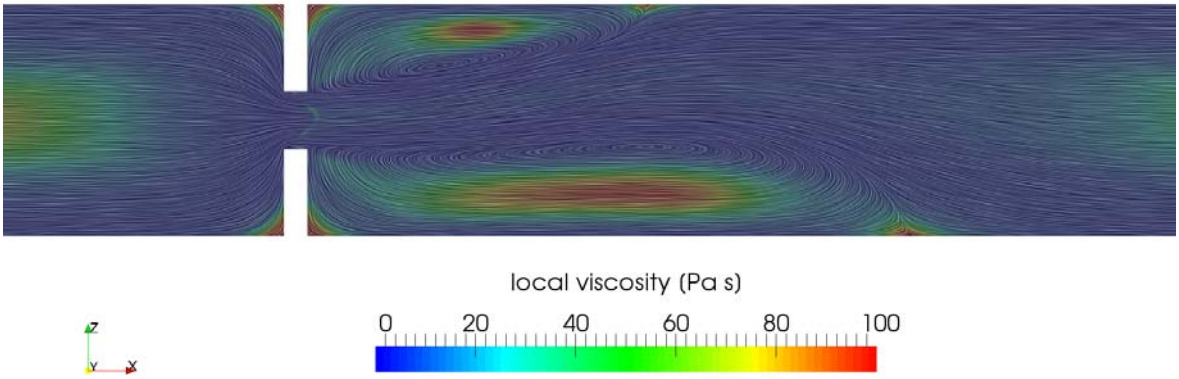

Figure 6: Orifice flow of the shear-thinning Carreau fluid, flow field visualisation using LIC applied to the velocity field, contour plot of the colour-coded local viscosity

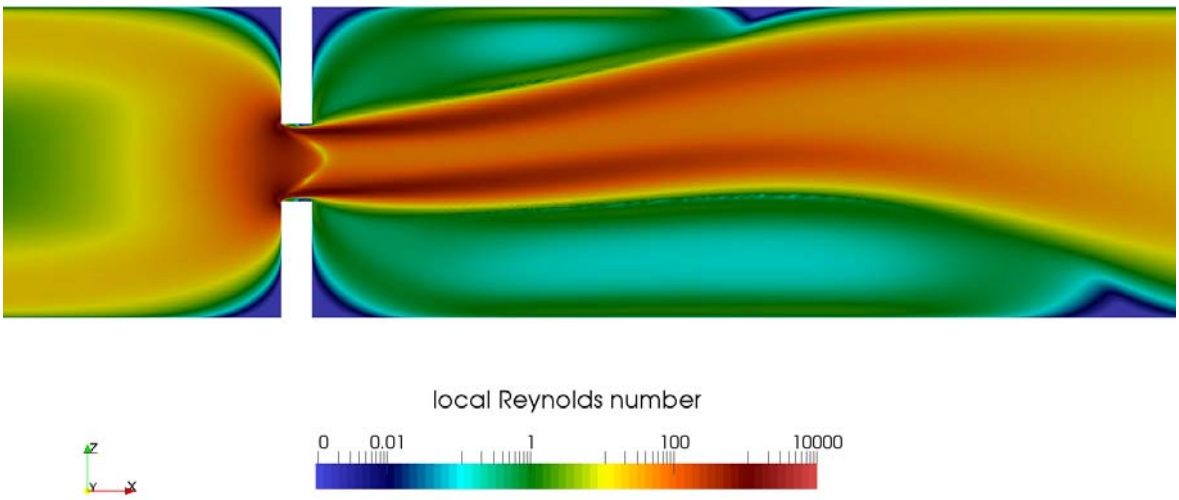

Figure 7: Orifice flow of the shear-thinning Carreau fluid, flow field visualisation using LIC applied to the velocity field, contour plot of the colour-coded local Reynolds number

behind, thus, disturbances can now be enforced and are able to deflect the jet flow. Once the deflected jet flow has hit the wall it stays attached at the wall due to the well-known Coanda effect. It has to be remarked, that at such high Reynolds numbers turbulence normally occurs. This could not be taken into account during this simulation campaign for several reasons: it not clear which transition mechanisms for these types of fluids and interface flows are appropriate, also the essential physical properties of turbulence under the condition of strong Reynolds number gradients are not clear, i.e. the turbulent length scales, the production and dissipation rates. This is a very challenging research field.

3.2 The Thermo-viscous Orifice Jet Flows

Now the impact of locally generated heat due to dissipation is taken into account. Other thermal loads are excluded, thus, the flow simulation results allow to evaluate the significance of dissipation related heat on the flow structure. It has to be remarked, that only the flow simulation result of the Newtonian fluid is shown. The flow field of the Carreau fluid reveals that thermal loads due to dissipation have a far less impact on the viscosity than shear-thinning itself, thus, the resulting Carreau fluid flow structure is very similar to that depicted in figure 7.
Now, the Newtonian fluid viscosity is allowed to change depending on that temperature, which is locally acting on the fluid. However, the temperature dependence of the fluid has to be modelled: the decision was made to use the same thermo-viscosity model as for the Carreau fluid, see equation (3). Of course, such a model might not be realistic for Newtonian fluids, however, in the sense of a numerical experiment this approach shall facilitate to unfold the physical reason of the symmetry breaking of the orifice jet flow. The impact of dissipation generated heat

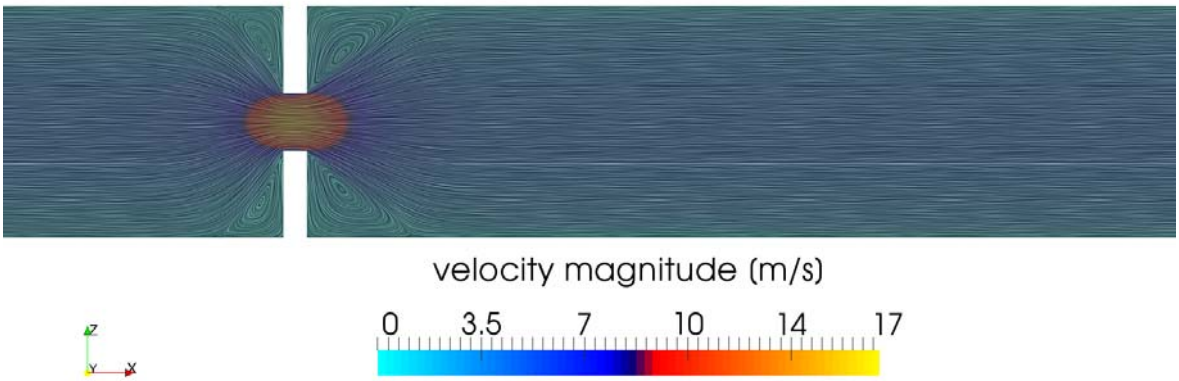

Figure 8: Orifice flow of the thermo-viscous Newtonian fluid affected by thermal loads due to dissipation, flow field visualised using LIC applied to the velocity field, contour plot of the colour-coded velocity magnitude

on the flow field is illustrated in figure 8, obviously the Moffatt corner vortices at the orifice plate are significantly enlarged, now reaching the size of the orifice itself. Consequently, the separation and attachment points are shifted away from the orifice. Furthermore, in contrast to the pure isothermal case, now, outwards curved vortical bubbles can be identified. This is a hint

that the local Reynolds number has been changed significantly by introducing thermal load due to dissipation. This is illustrated in figure 9, obviously the corner vortices are dissipating most energy at their borders to the spreading orifice jet flow, here the local Reynolds numbers are dropping, which leads to the vortex enlargement.

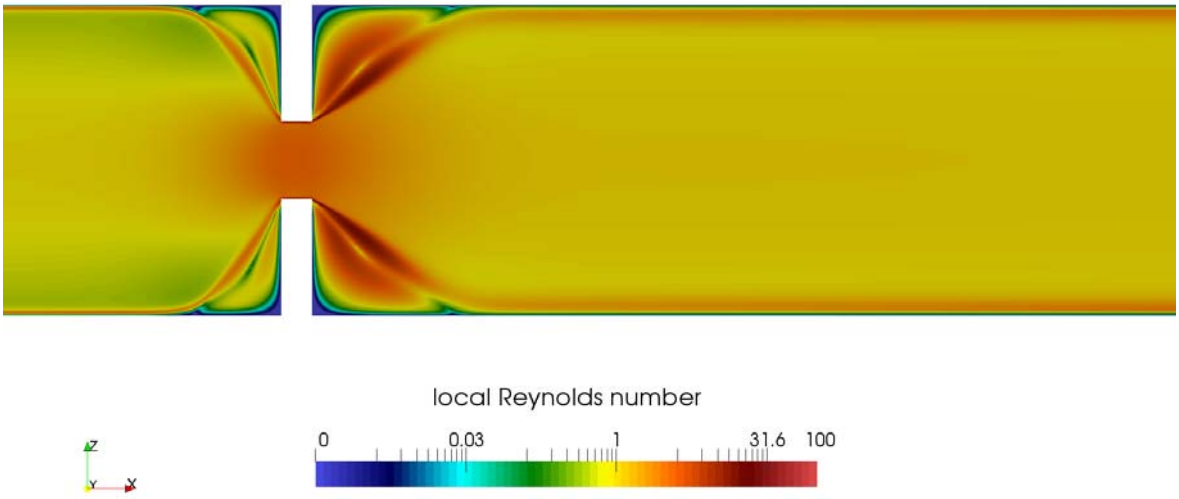

Figure 9: Orifice flow of the thermo-viscous Newtonian fluid affected by thermal loads due to dissipation, contour plot of the colour-coded local Reynolds number is shown

3.3 Control of the Thermo-Viscous Shear-Thinning Orifice Jet Flow

The observation that generated heat can change the viscosity of Newtonian and non-Newtonian fluids significantly, leads to the idea to control the orifice jet flow by introducing artificial heat. Therefore, the walls of the outflow channel are heated. The resulting heat transfer into the fluid is varied by setting different wall temperatures. Although slight effects are also expected for the Newtonian fluids, here, the Carreau fluid flow cases are the focal point of the investigation. At first the only the upper wall of the outflow channel is heated, setting a wall temperature of $463.15K$, all other temperatures, channel wall and the fluid temperatures at the entry, remain at $403.15K$. The drastically changed flow topology is depicted in figure 10: Now, the orifice jet is deflected downwards. This new flow topology is not only a mirrored flow, the wall temperature leads to a significantly larger upper vortical flow separation structure and a drastically decreased lower vortical separation bubble. The reason is that the near wall temperature induced by heat transfer from the wall reduces the viscosity to significantly lower levels in comparison to the pure shear-thinning flow case. Eventually, there are fewer momentum losses at the upper wall leading to two effects: The flow attachment point is shifted downstream and the vortical flow of the separation bubble is able to accumulate more momentum which is turned into angular momentum. Due to enforced lower viscosity levels the overall energy dissipation is decreased, which allows the vortical flow structure to grow more than expected. In contrast to the pure

isothermal orifice flow, the deflected orifice flow with its larger and smaller vortical separation bubbles reveals a strong unsteady flow behaviour. In fact the upper separated flow region contains up to four independent sub-vortices. These intermittent sub-vortices are structurally changing over time, they are fusing and splitting again and again. Also the smaller separation bubble reveals sub-vortices, but only two more or less stable sub-vortices. The impact of

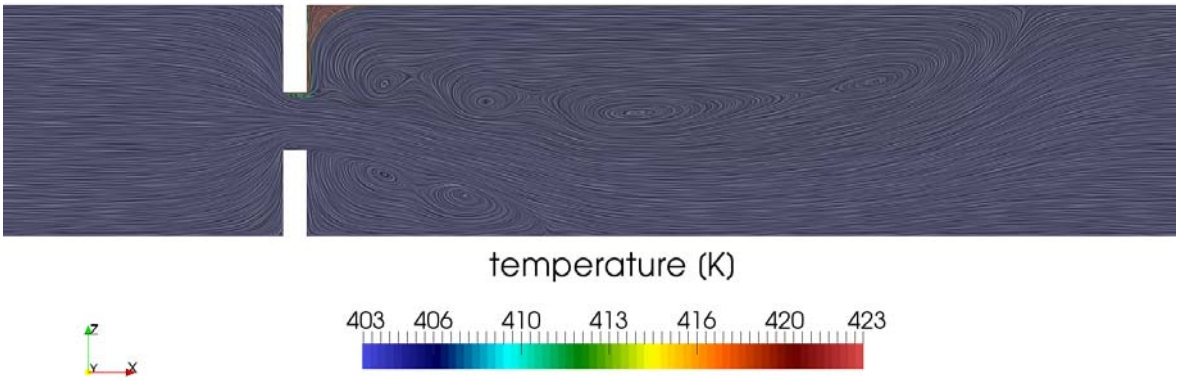

Figure 10: Orifice flow of the thermal viscous shear-thinning Carreau fluid, heated upper wall of the outflow channel, flow field visualisation using LIC applied to the velocity field, contour plot of the colour-coded local temperature

dissipation and the increased temperature of the upper wall of the outlet channel can also be observed in figure 11, following the contour plot of the local viscosity-temperature shift factor. Obviously the essential mechanisms are, first, the heat transfer at the upper wall of the outlet channel which drastically reduces the local viscosity close to the wall, thereby also reducing the energy and momentum loss of the reverse flow, and secondly, the convectional transport of heat due to the vortical flow towards the rear orifice wall and its impact on the flow separation at the orifice passage itself. There, the heated fluid at the orifice reveals a lower wall friction and more crossflow momentum, thus, separation is enforced. Furthermore, the combination of high shear rates with the additionally introduced thermal loads are decreasing the viscosity so much that the formerly steady flow state is transformed into a highly unsteady flow state. A ponderable global impact on the flow topology can be observed: the orifice jet flow is pushed by pulsatively oscillating separating flow, and, additionally, spot-like regions with a lower local viscosity-temperature shift factor at the upper border of the orifice jet flow are floating downstream indicating locally heated fluid.
From the observation, that local heat transfer is able to change the flow topology significantly, it might be deduced that control of local hear transfer allows to control the orifice jet flow deflection. In this study this was investigated by the following numerical experiment: the lower and upper walls of the outlet channel are differently heated, in the first variant, the upper wall temperature is set to $T_o = 423.15K$ and the lower wall temperature to $T_u = 483.15K$, in the second case vice versa. Note that not only the global heat transfer is increased due to heating both walls, also the temperature level is increased by $20K$.
At the first glance the new flow structure is similar to that of the isothermal Carreau fluid flow

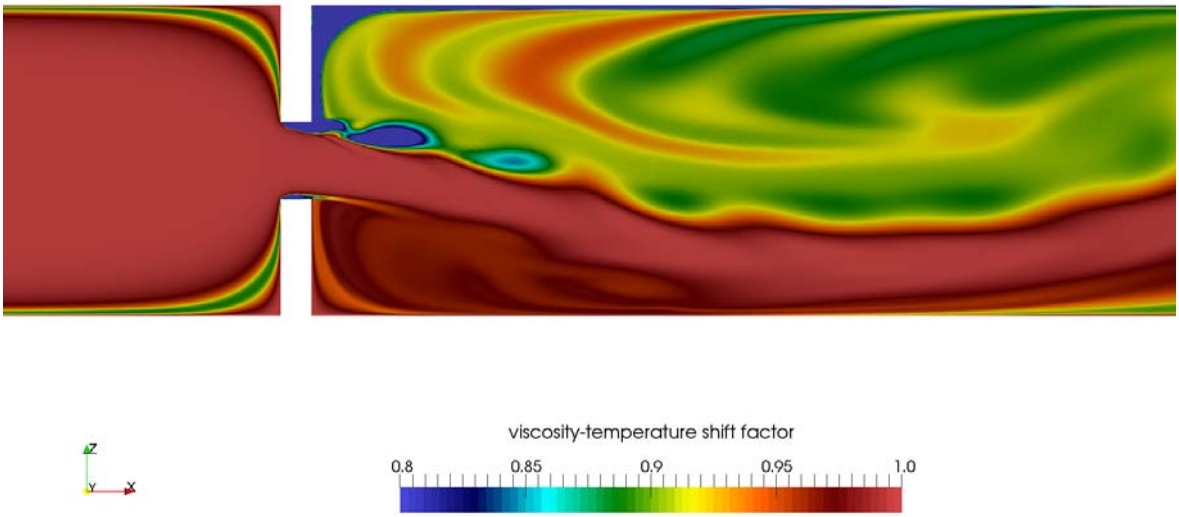

Figure 11: Orifice flow of the thermal viscous shear-thinning Carreau fluid, heated upper wall of the outflow channel, contour plot of the colour-coded local viscosity-temperature shift factor, magnified grid cut view

case, it also shows an upwards deflected orifice jet flow, however, the core jet flow is swaying with strong oscillations at its borders. The reverse flow regions are a bit larger and they reveal more small interchanging temporally growing and decaying sub-vortices. An impression of these dominant structures is given in figure 12. The mechanisms behind is the same: the higher wall temperatures are decreasing the near wall viscosity, momentum losses are decreased, which leads to increased flow separation bubbles containing intermittent sub-vortices. In variant 2 the wall temperatures are flipped: now the lower wall temperature is set to $T_u = 423,15K$ and the upper wall temperature to $T_o = 483,15K$. Thus, the global wall temperature gradient has been inverted, and, therewith, also the orifice jet flow, which is now deflected downwards. Besides this global flow behaviour, some characteristic flow features are remaining the same: first, the unsteadiness of the jet flow, in particular at the jet borders, where wavy-like small hot spots are fading away, and secondly, the transient behaviour of sub-vortices within the separated reverse flow region. Figure 13 allows to compare the flow structures. When comparing the one-wall heated case with the last two flow cases it is evident that increased heat transfer and the higher wall temperature level leads to longer reverse flow regions.

4 Conclusion

In this numerical simulation study the flow of a thermo-viscous shear thinning Carreau fluid trough a channel with an orifice plate has been investigated. It has been demonstrated, that the Carreau fluid viscosity property of shear-thinning is responsible for changing the orifice jet flow topology, the jet flow is deflected, the symmetry observed in case of Newtonian fluids is broken. Furthermore, it has been demonstrated that additional thermal loads introducd by

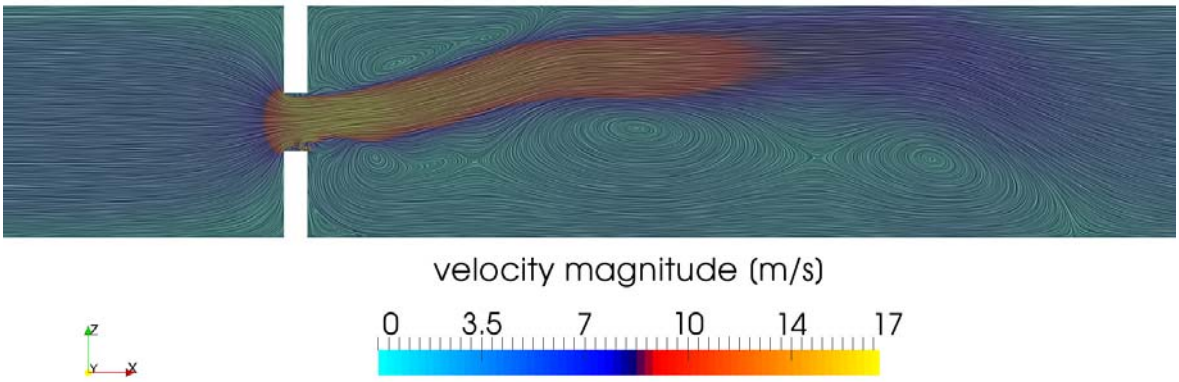

Figure 12: Variant 1: orifice flow of the thermal viscous shear-thinning Carreau fluid, heated lower and upper wall of the outlet channel, $T_u = 483K$ and $T_o = 423K$, contour plot of the colour-coded velocity magnitude, magnified grid view

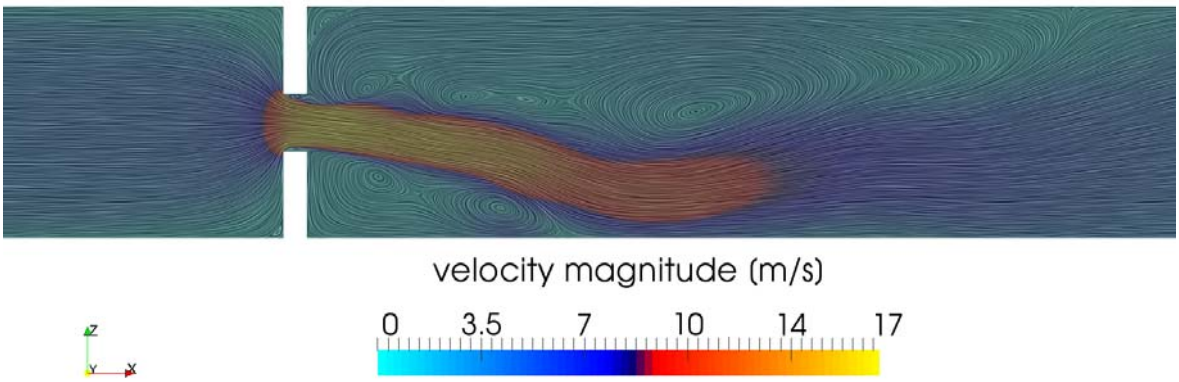

Figure 13: Variant 2: orifice flow of the thermal viscous shear-thinning Carreau fluid, heated lower and upper wall of the outlet channel, $T_u = 423K$ and $T_o = 483K$, contour plot of the colour-coded velocity magnitude, magnified grid view

heat transfer are also able to change the flow regime from steady state to an highly unsteady regime. Furthermore, it has been observed that the thermal-viscous shear-thinning Carreau fluid is very sensitive to local heat transfer, this has led to the interesting idea to control the flow structure by inducing additional heat. This has been realized by heating up the outlet channel walls. The physical mechanism behind the flow control concept has been identified: It can be recapitulated that in case of a sufficiently high wall temperature difference between a hot and a cold wall the orifice jet flow jet is deflected to the cooler wall following the global heat transfer direction. The thermal property of the shear-thinning Carreau fluid with its strong sensitivity to higher temperatures is the reason. The increased heat transfer generates high thermal loads, which lowers the viscosity of the fluid exceedingly, but also reduces dissipation and momentum loss. Hence, the reverse flow is able to transport more hotter fluid with higher momentum back to the orifice. At the orifice separation location the cross flow of the hotter fluid, which is induced by the reverse flow at the orifice backplane, is able to deflect the jet flow more than its colder counterpart due to its higher momentum. This deflection leads to the different size of the Moffatt type separation bubbles. Consequently, the larger one is able to accumulate more hotter fluid, therefore, it can grow more and more up to a certain limit. This thermal-viscosity - shear thinning - fewer momentum loss feedback mechanism is responsible for enlarging the vortical separation bubble.
There are some questions which have not been answered so far: In this investigation only a certain geometrically fixed orifice configuration was given, a parametric study is missing, since the flow separation behaviour of the orifice jet flow depends on the orifice aspect ratio and orifice / channel relation. There are also dependencies on wall temperature differences, which in fact, have been used for the performed flow control, but, a sensitivity study is still missing, which might allow to limit the additional heat introduced at the walls. A systematic parameter variation would enable to derive a multi parametric flow control map, which could be applied to technical applications. Therefore, there is enough research work left for the future.

Acknowledgment

The authors would like to thank the German Aerospace Center (DLR) and the University of Kassel for greatly supporting this research work.

REFERENCES

[1] Alves, M. A., Oliviera, P. J. and Pinho, F. T.: Benchmark solutions for the flow of Oldroyd-B and PTT fluids in planar contractions. Journal of Non-Newtonian Fluid Mechanics, Vol. 110, pp. 45-75, 2003.

[2] Alvi, S. H., Sridharan, K., and Lakshmana R. N. S.: Loss Characteristics of Orifices and Nozzles. ASME J. Fluids Eng., 100 (3), pp. 299307, 1978.

[3] Andrade, E. N. D.: A theory of the viscosity of liquids. part 1. Philosophical Magazine, Vol. 17, pp. 497-511, 1934.

[4] Battaglia, F. and Papadopoulous, G.: Bifurcation characteristics of flows in rectangular

sudden expansion channels. J. Fluids. Engg., Vol. 128, pp. 671-679, 2006.

[5] Bird, R. B.: Non-Newtonian behavior of polymeric liquids. Physica A: Statistical and Theoretical Physics, Vol. 118, No. 1–3, pp. 3-16, 1983.

[6] Bird, R. B., Curtiss, C. F.: Nonisothermal polymeric fluids. Rheol. Acta, Vol. 35, pp. 103-109, 1983.

[7] Bird, R. B., Hassager, O.: Dynamics of Polymeric Liquids: Vol.1: Fluid Mechanics. Series: Dynamics of Polymeric Liquids, London, New York, John Wiley & Sons, 1987.

[8] Carreau, P. J.: Rheological equations from molecular network theories. J. Rheol., Vol. 16, No. 1, pp. 99-127, 1972.

[9] Chabral, B.; Leedom, L. C.: Imaging Vector Fields Using Line Integral Convolution. In: Proceedings of SIGGRAPH 93. pp. 263-270, New York, 1993.

[10] CentaurSoftware, http://www.centaursoft.com.

[11] Cherdron, W., Durst, F. and Whitelaw, J. H.: Asymmetric flows and instabilities in symmetric ducts with sudden expansions. J. Fluid. Mechanics, Vol.84, pp. 13-31, 1978.

[12] Cogswell, F. N.: Converging flow of polymer melts in extrusion dies. Polymer Engg Sci., Vol. 1, pp. 64-73, 1972.

[13] Cogswell, F. N.: Converging flow and stretching flow: a compilation. J. Non-Newtonian Fluids, Vol. 4, pp. 23-38, 1978.

[14] Drikakis, D.: Bifurcation phenomena in incompressible sudden expansion flows. Phys. Fluids, Vol. 9, pp. 77-87, 1997.

[15] Durst, F., Melling, A. and J.H. Whitelaw, J.H.: Low Reynolds number flow over a plane symmetrical sudden expansion. J. Fluid. Mechanics, Vol. 64, pp. 111-128, 1974.

[16] ESDU International PLC, Incompressible Flow Through Orifice Plates – A Review of the Data in the Literature, Data Item No. TN 07007, 2007.

[17] Evans, R. E.and K. Walters, K.: Flow characteristics associated with abrupt changes in flow geometry in the case of highly elastic liquids. Journal of Non-Newtonian Fluid Mechanics, Vol. 20, pp. 11-29, 1986.

[18] Fearn, R., Mullin, T. and Cliffe, K.: Non-linear flow phenomena in a symmetric sudden expansion. J. Fluid Mech., Vol. 211, pp. 595-608, 1990.

[19] Ferry, J. D.: Viscoleastic Properties of Polymers. Third edition, New York; John Wiley & Sons, 1980.

[20] Greenspan, D.: Numerical Studies of Viscous, Incompressible Flow through an Orifice for Arbitrary Reynolds Number. International Journal for Numerical Methods in Engineering, Vol. 6, pp. 489-496, 1973.

[21] Johansen, F. C.: Flow through Pipe Orifices at Low Reynolds Numbers. Proceedings of the Royal Society of London, Series A, Vol. 126, Issue 801, pp. 231-245, 1930.

[22] Knopp, T., Zhang, X., Kessler, R. and Lube, G.: Enhancement of an industrial finite-volume code for large-eddy-type simulation of incompressible high Reynolds number flow using near-wall modelling. Journal of Computer Methods in Applied Mechanics and Engineering, Vol. 199, pp. 890-902, 2010.

[23] Lakshmana, R. N. S., Sridharan, K., and Alvi, S. H.: Critical Reynolds Number for Orifice and Nozzle Flows in Pipes. J. Hydraul. Res., 15 (2), pp. 167178, 1977.

[24] Moffatt, H.: Viscous and resistive eddies near a sharp corner. Journal of Fluid Mechanics, Vol. 18(1), pp. 1-18. doi:10.1017/S0022112064000015, 1964.

[25] Neofytou, P.: Transition to asymmetry of generalized newtonian fluid flows through a symmetric sudden expansion. J. Non-Newtonian Fluid Mech., Vol. 13, pp. 132-140, 2006.

[26] Niedziela, D.: On numerical simulations of viscoelastic fluids. Dissertation. University of Kaiserslautern, Kaiserslautern, 2006.

[27] Ostwald, W.: Ueber die rechnerische Darstellung des Strukturgebietes der Viskosität, Kolloid Zeitschrift, Vol. 47 (2), pp. 176-187, 1929.

[28] Owens, R. G., Phillips, T. N.: Computational Rheology. Computational Rheology. Imperial College Press, ISBN 9781860941863, 2002.

[29] Rodd, L., Scott, T. P., Boger, D. V., Copper-White, J. J. and McKinley, G. H.: The inertioelastic planar entry flow of low-viscosity elastic fluids in micro-fabricated geometries. Journal of Non-Newtonian Fluid Mechanics, Vol. 129, pp. 1-22, 2005.

[30] Rothstein, J. P. and McKinley G. H.: Extensional Flow of a Polystyrene Boger Fluid through a 4:1:4 Axisymmetric Contraction/expansion." Journal of Non-Newtonian Fluid Mechanics, Vol. 86, pp. 61-88, 1999.

[31] Shima, N.: Loss and Discharge Characteristics of a Flow of Polymer Solutions Through Pipes Orifices. Bull. JSME, 27 (225), pp. 443-449, 1984.

[32] Skelland, A. H. P.: *Non-Newtonian flow and heat transfer*, John Wiley & Sons, New York, 1967.

[33] Ternik, P.: Planar sudden symmetric expansion flows and bifurcation phenomena of purely viscous shear-thinning fluids. J. Non-Newtonian Fluid Mech., Vol. 157, pp, 15-25, 2009.

[34] Ternik, P.: New contributions on laminar flows of inelastic non-newtonian fluid in the two-dimensional symmetric expansion: Creeping ans slowly moving flow conditions. J. Non-Newtonian Fluid Mech., Vol. 165, pp. 1400-1411, 2009.

[35] Valle, D. D. , Tanguy, P. A . and Carreau, P. J.: Characterization of the Extensional Properties of complex fluids Using an Orifice Flowmeter. Journal of Non-Newtonian Fluid Mechanics, Vol. 9, pp. 1-13, 2000.

[36] Wendt, J. F. (Ed.): Computational Fluid Dynamics - An Introduction. Third edition, Berlin, Heidelberg; Springer, 2009.

[37] White, S. A., Gotsis, A. D. and Baird, D. G.: Review of the entry flow problem: Experimental and numerical. Journal of Non-Newtonian Fluid Mechanics, Vol. 24, pp. 121-160, 1987.

[38] Williams M. L., Landel, R. F. and Ferry, J. D.: The temperature dependence of relaxation mechanisms in amorphous polymers and other glass-forming liquids. *Journal of the American Chemical Society*, Vol. 77, pp. 3701-3707, 1955.